Spectroscopic characterization of gold supported on tungstated zirconia

M. Kantcheva [a,*], M. Milanova [a], I. Avramova [b], S. Mametsheripov [a]

[a] Department of Chemistry, Bilkent University, 06800 Bilkent, Ankara, Turkey
[b] Institute of General and Inorganic Chemistry, Bulgarian Academy of Sciences, Sofia 1113, Bulgaria

ARTICLE INFO

ABSTRACT

Gold catalysts supported on tungstated zirconia (containing 5–20 wt% WO$_3$) are prepared by cationic adsorption from aqueous solution of [Au(en)$_2$]Cl$_3$ complex. The materials are characterized by XRD, DR-UV–vis spectroscopy and XPS. The nature of the deposited gold species is studied by FT-IR spectroscopy of adsorbed CO. It is concluded that the gold particles occupy preferentially the WO$_x$-free zirconia surface and the dispersion of gold depends on the amount of coodinatively unsaturated (cus) Zr^{4+} ions. Modification of zirconia by tungsten increases the gold uptake but at the same time causes decrease in the concentration of (cus) Zr^{4+} ions thus lowering the dispersion of gold clusters. According to the results of in situ FT-IR spectroscopy, the Au/WO$_x$–ZrO$_2$ catalysts display higher activity in the CO oxidation in the low-temperature range (up to 150 °C) than the WO$_x$-free Au/ZrO$_2$ sample. The low-temperature activity of the W-containing catalysts could be associated with decreased basicity of the support oxide ions resulting in reduced accumulation of stable carbonate species.

© 2012 Elsevier B.V. All rights reserved.

1. Introduction

Supported gold catalysts are highly active in reactions important for the environmental catalysis [1], in particular for low-temperature CO oxidation [1–9]. Crucial factors that control the activity of gold catalysts are the metal particle size, the nature and particle size of the oxide support, and the structure of Au-oxide contacts [1]. The practical application of gold catalysts, however, is hindered because of their tendency for deactivation with the operation time. The most probable reason for the decrease in the catalytic activity is the formation of stable carbonate species which block the perimeter of gold–support interface considered as active reaction zone [3–6]. The accumulation of CO$_x$ species on the catalyst surface during the course of CO oxidation takes place by readsorption of CO$_2$ product molecules [5]. Since CO$_2$ is an acidic molecule, lowering of the basicity of the support surface by introduction of an acidic component would prevent the formation or reduce the amount of stable carbonate species.

Highly dispersed (2–5 nm) gold particles on oxide supports can be obtained by deposition–precipitation (DP) using HAuCl$_4$ as a gold precursor [1]. However, this method cannot be applied in the case of acidic oxide supports with a point of zero charge (PZC) below 5 such as silica or WO$_3$ [1]. This is because the support surface is negatively charged above the PZC which does not allow strong interaction between the support and the anionic gold precursor

(AuCl$_4$$^-$). Cationic exchange is presumed to be an effective way of introducing gold into acidic oxides, e.g. SiO$_2$-based supports [8–12].

Herein, we report the results of characterization of gold catalyst supported on tungstated zirconias. The Au/WO$_x$–ZrO$_2$ samples were prepared by cationic adsorption using [Au(en)$_2$]Cl$_3$ as the precursor (en = ethylenediamine). This method was developed first by Guillemot et al. [10] for the introduction of gold into Y zeolites and used also by others [8,9,11] for deposition of gold on silica. In order to evaluate the potential of a new material as a catalyst in the process of CO oxidation, it is important to investigate the interaction of the reactants with the surface. For that purpose we used in situ FT-IR spectroscopy to study the adsorption of CO and its coadsorption with oxygen over Au-promoted and Au-free zirconia and tungstated zirconias.

2. Experimental

2.1. Sample preparation

Two different procedures were used for preparation of hydrated zirconia. According to procedure 1, hydrated zirconia (denoted as HZ-1) was prepared by hydrolysis of 0.3 M solution of zirconyl chloride (ZrOCl$_2$·H$_2$O, Aldrich) with concentrated (25%) ammonia solution at pH 9. The slurry of the precipitated material was kept for aging at room temperature for 12 h. Then the product was separated by vacuum filtration, redispersed in deionized water, washed thoroughly to remove the chloride ions and dried at 100 °C. The crystallographic structure of the material obtained after calcination at 600 °C was predominantly monoclinic zirconia. Tungstated

* Corresponding author.
E-mail address: margi@fen.bilkent.edu.tr (M. Kantcheva).

Table 1
Sample notation, BET surface areas, nominal tungsten and analytical gold contents.

Sample	S_{BET} (m²/g)	WO₃ (wt%)	Wᵃ (at/nm²)	Au loading (wt%)	Au loading (at %)	Au particle size (nm)ᵇ
Au/ZrO₂	143	–	–	1.43 ± 0.03	0.30	8
Au/5WZ-I	116	5.0	1.2	1.27 ± 0.01	0.27	8
Au/12WZ-I	115	11.8	3.0	1.83 ± 0.01	0.40	9
Au/20WZ-I	140	19.4	4.5	2.06 ± 0.03	0.44	10
Au/18WZ-CP	118	18.0	4.8	2.27 ± 0.01	0.48	10

ᵃ The W surface density is calculated based on the weight of zirconia.
ᵇ According to XRD.

zirconia was synthesized by coprecipitation [13] with nominal content of 18 wt% WO₃ and by impregnation of HZ-1 with aqueous solution of ammonium metatungstate (AMT, Fluka) using the method proposed by Martinez et al. [14]. This procedure consisted of impregnation of HZ-1 with aqueous solution (3 mL/g hydrated zirconia) containing the required amount of AMT to obtain WO₃ loadings corresponding to 5, 12 and 20 wt%. The final calcination temperature of all tungstated zirconias was 600 °C. Gold was deposited by cation adsorption for 2 h from aqueous solution of $[Au(en)_2]^{3+}$ complex (5.85 × 10⁻³ M) at pH = 9.6 and room temperature. After the separation of the gold complex solution by filtration, the solid was washed by deionized water until negative test for chloride ions. The samples were dried at 80 °C for 48 h and calcined for 1 h at 400 °C. The cationic gold precursor was prepared following the procedure of Block and Bailar [15]. The obtained materials were labeled as Au/xWZ-CP or I, where x stands for the WO₃ nominal content in wt%. CP and I denote co-precipitation and impregnation, respectively (see Table 1).

In order to study the effect of tungsten, gold was deposited also on zirconia by cation adsorption of $[Au(en)_2]^{3+}$ complex using the same conditions applied to the W-containing samples. Since the incorporation of WO_x species stabilizes the tetragonal phase of zirconia [14,16–22], WO_x-free tetragonal zirconia was used for the preparation of ZrO₂-supported gold sample. The goal was to eliminate the effect of crystal phase on the interaction of gold precursor with the support because there are differences in the acid–base properties [23], and types and concentration of the surface hydroxyl groups [24] of zirconia polymorphs. In addition, the CO adsorption capacity of monoclinic zirconia is larger than that of the tetragonal phase [23] which may affect the CO + O₂ surface reaction. Li et al. [25] have found that Au supported on monoclinic zirconia exhibited much higher activity in the low-temperature WGS reaction than the catalyst supported on tetragonal zirconia. Tetragonal phase of zirconia was prepared by a method similar to that described by Jung and Bell [24] denoted as procedure 2. The synthesis consisted of hydrolysis of 0.6 M solution of ZrO₂Cl₂·8H₂O with concentrated ammonia solution (25%) at pH = 9 and room temperature. The obtained precipitate was washed several times with deionized water until negative test for Cl⁻ ions. Then the washed precipitate was aged in aqueous solution of ammonia (with pH = 9) at 100 °C for 48 h under reflux and periodical supplement of NH₃(aq) in order to keep constant pH of 9. The resultant hydrated zirconia was dried at 100 °C for 24 h. The material was denoted as HZ-2. Tetragonal zirconia was obtained by calcination of the hydrated zirconia HZ-2 at 600 °C for 6 h.

2.2. Sample characterization

XRD analysis was performed on a Rigaku Miniflex diffractometer with Ni-filtered Cu Kα radiation (λ = 1.5405 Å). The DR-UV–Vis spectra were obtained under ambient conditions with a fiber optic spectrometer AvaSpec-2048 (Avantes) using WS-2 as a reference. The BET surface area measurements were performed with a TriStar 3000 automated gas adsorption analyzer (Micrometrics). The samples were dehydrated under vacuum (10⁻² Torr) for 3 h at 250 °C

before the measurements in order to remove adsorbed water and volatile compounds.

The content of gold was determined by ICP-MS analysis. The tungsten content in the samples was calculated as difference between the nominal content in the solid and the concentration of tungsten in the filtrate produced during the deposition of gold from the gold precursor. The tungsten content in the filtrate was determined spectrophotometrically by the thiocyanate method at λ = 410 nm [20,26,27].

The X-ray photoelectron spectra were obtained using un-monochromatized Al Kα (1486.6 eV) radiation in a VG ESCALAB MK II electron spectrometer under base pressure of 1 × 10⁻⁸ Pa. The spectrometer resolution was calculated from the Ag 3d₅/₂ line with the analyzer transmission energy of 20 eV. The half-width of this line was 1 eV. The spectrometer was calibrated against the Au 4f₇/₂ line (84.0 eV) and the sample charging was estimated from C 1s (285 eV) spectra from natural hydrocarbon contaminations on the surface. The accuracy of the BE measured was 0.2 eV. The photoelectron spectra of C 1s, O 1s, Zr 3d, W 4f and Au 4f were recorded and corrected by subtracting a Shirley-type background and quantified using the peak area and Scofield's photoionization cross-sections. The Au particle size was obtained from the XPS peak intensity treated according to the Kerkhof–Moulijn model [28,29].

The FT-IR spectra were recorded using a Bomem Hartman & Braun MB-102 model FT-IR spectrometer with a liquid-nitrogen cooled MCT detector at a resolution of 4 cm⁻¹ (100 scans). The self-supporting discs (∼0.01 g/cm²) were activated in the IR cell by heating for 1 h in a vacuum at 400 °C, and in oxygen (100 Torr, passed through a trap cooled in liquid nitrogen) at the same temperature, followed by evacuation for 1 h at 400 °C. The spectra of adsorbed gases were obtained by subtracting the spectra of the activated sample from the spectra recorded. The sample spectra were also gas-phase corrected.

3. Results and discussion

3.1. Structural characterization

According to the XRD data (Fig. 1) all of the samples studied (except Au/5WZ-I) have the structure of tetragonal zirconia (ICDD Cart No. 04-005-4479). The Au/5WZ-I sample contains small amount of monoclinic zirconia (ICDD Cart No. 00-013-030).

With increase in the tungsten loading, the analytical content of gold increases (Table 1). It is well known that tungstated zirconia contains acidic protons and their amount increases with the surface density of the WO_x species [13,16–20,30]. It is reasonable to propose that as higher the concentration of acidic hydroxyls on the support surface as larger the amount of deprotonated M–O⁻ surface sites (M = W and Zr) thus leading to greater number of anchoring sites for the $[Au(en)_2]^{3+}$ complex resulting in higher surface concentration of gold. The average size of gold particles, calculated by using Scherrer equation and the main gold diffraction line of 2θ = 38.2° (ICDD Cart No. 00-004-0784), increases with the W content (Table 1).
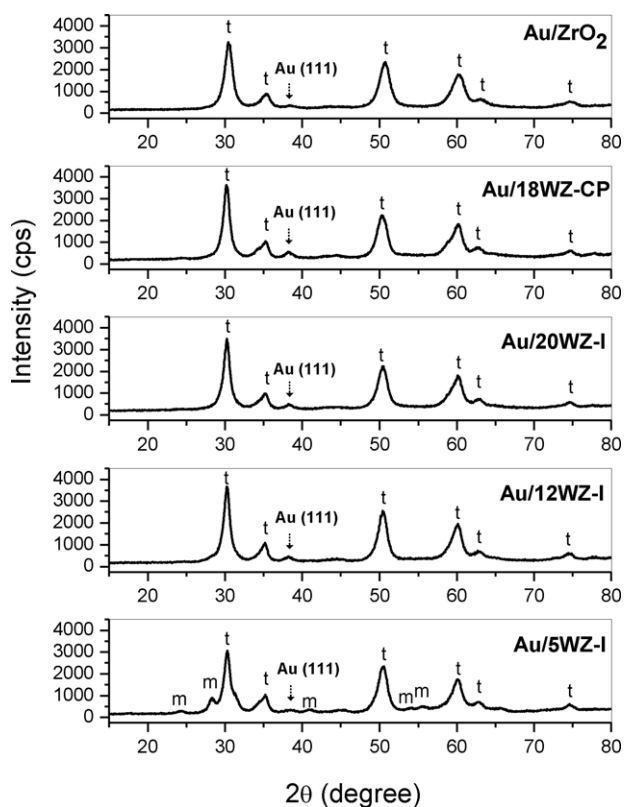
Fig. 1. XRD patterns of the samples studied (t: tetragonal; m: monoclinic).

The basic medium used for the $[Au(en)_2]^{3+}$ adsorption caused some leaching of WO_x species only in the case of Au/12WZ-I and Au/20WZ-I samples. After the deposition of gold, the tungsten loss amounts to 0.20 ± 0.05 and 0.61 ± 0.02 wt% of WO_3 for Au/12WZ-I and Au/20WZ-I, respectively.

3.2. DR-UV–vis spectra

Fig. 2 compares the optical spectra of the samples studied. The absorption band at 293–270 nm with a shoulder at 260 nm observed in the spectra of the Au-free samples (Fig. 2, spectra (a)) corresponds to LMCT ($O^{2-} \rightarrow W^{6+}$) transition in oligomeric WO_x species with different degree of polymerization [14,17–21]. The introduction of gold causes drastic change in the optical spectra (Fig. 2, spectra (b)). The broad absorption with maximum at 550 nm observed on the gold-containing samples is characteristic of the plasmonic oscillation mode of nanosized gold particles [11,31,32]. The strong band at 270–293 nm has disappeared and weak signals at 225–230 and 260–275 nm are observed instead. Based on the spectrum of Au/ZrO₂ sample (Fig. 2A, spectrum (c)), the former band is attributed to the $O^{2-} \rightarrow Zr^{4+}$ CT transition. The spectra of the Au-containing samples indicate that gold hinders the detection of LMCT transitions. Due to the high absorption coefficient of gold particles [33], the support cannot interact with the radiation. Consequently, the fundamental bands of tungstated zirconia are detected with significantly lower intensities.

3.3. XPS analysis

The results of XPS analysis for all samples are summarized in Table 2. Binding energy of Au $4f_{7/2}$ is around 82.8–83.5 eV which, in agreement with the literature data on Au/ZrO₂ catalysts [7,25,34–36], is assigned to metallic gold. The full width at half maximum (FWHM) of Au 4f photoelectron line decreases with

increasing the WO_3 content. This is a sign of more uniform distribution of Au particles on the W-modified sample surfaces most likely due to the increased gold uptake. The reason for the formation of metallic gold without additional reduction step is the low thermal stability of the $[Au(en)_2]^{3+}$ precursor complex when adsorbed on oxide surfaces [10,11,37]. The initial color of the samples was light yellow, however, during the drying at 80 °C the samples became gray-black. The change in the color was faster for the samples with higher W content, which suggests that tungsten assists in the decomposition of gold precursor complex.

Since the XRD data provide information about the size of large gold clusters (larger than 5 nm [38]), the size of the gold particles was estimated by XPS intensity ratios using the model proposed by Kerkhof and Moulijn [28]. This model is based on the metal loading and specific surface area of the catalysts and is useful for the characterization of very small metal particles [38]. The average particle size calculated from XPS for all gold containing samples is around 3 nm. These results indicate that large (8–10 nm) and small (~3 nm) gold particles are present on the surfaces of the samples prepared by cationic adsorption of the $[Au(en)_2]^{3+}$ precursor.

The spectra of the samples in the W 4f region contain intense doublet with W $4f_{7/2}$ line at 35.1–36.3 eV corresponding to W^{6+} [22,30]. The Zr 3d photoelectron line for all Au catalysts exhibits peak for Zr $3d_{5/2}$ at 182.0–182.9 eV, close to that observed for Zr^{4+} ions [25,30,34,36,39–41]. Fig. 3 shows that the W/Zr surface ratios for the gold catalysts supported on tungstated zirconia prepared by impregnation increases linearly as a function of the tungsten content. This suggests that the dispersion of the WO_x species on the surface of the gold catalysts is uniform [19,22]. For the Au/WZ-CP sample the calculated W/Zr surface atomic ratio deviates from the established linear dependence. It has been shown that all tungsten is located on the surface when tungstated zirconia was prepared by impregnation whereas using co-precipitation results in incorporation of W atoms into ZrO₂ lattice, stabilizing the tetragonal structure [16,30].

In the O 1s XPS region an intensive peak at ~530.4 eV is observed for all investigated catalysts. Small asymmetry at higher binding energy side is detected too. This second peak can be related to the existence of O^- ions [42]. This suggests the presence in the subsurface of oxygen ions that bear lower electron density than the "O^{2-}" ions; formally these oxide ions could be described as "O^-" species. They could be associated with sites having higher covalence of the M—O bonds and smaller coordination number of oxygen ions than a regular site. A reasonable hypothesis is to consider the existence, in variable proportions, of defects in the subsurface.

The results in Table 2 show that the method of introduction of WO_x species to zirconia (coprecipitation versus impregnation) does not affect the surface concentration of gold. However, in agreement with the chemical analysis, the amount of gold on the surface increases with the WO_3 loading.

3.4. In situ FT-IR spectroscopy

3.4.1. FT-IR spectra of the activated samples

Fig. 4 compares the spectra of the activated Au-free and Au-containing xWZ-I samples. In the OH stretching region all samples of tungstated zirconia contain a band at 3640–3635 cm^{-1} which is attributed to W—OH groups [20]. The broad absorption at approximately 3445 cm^{-1} indicates the presence of H-bonded hydroxyls. The spectra in the fundamental W=O stretching region show a sharp band at 1008–1002 cm^{-1} typical of W=O species [17,19–21]. The deposition of gold does not cause perturbation of the W=O band. However, compared to the xWZ-I supports, all Au-containing samples display bands in the OH stretching region with lower intensities. This is associated with the involvement of the surface
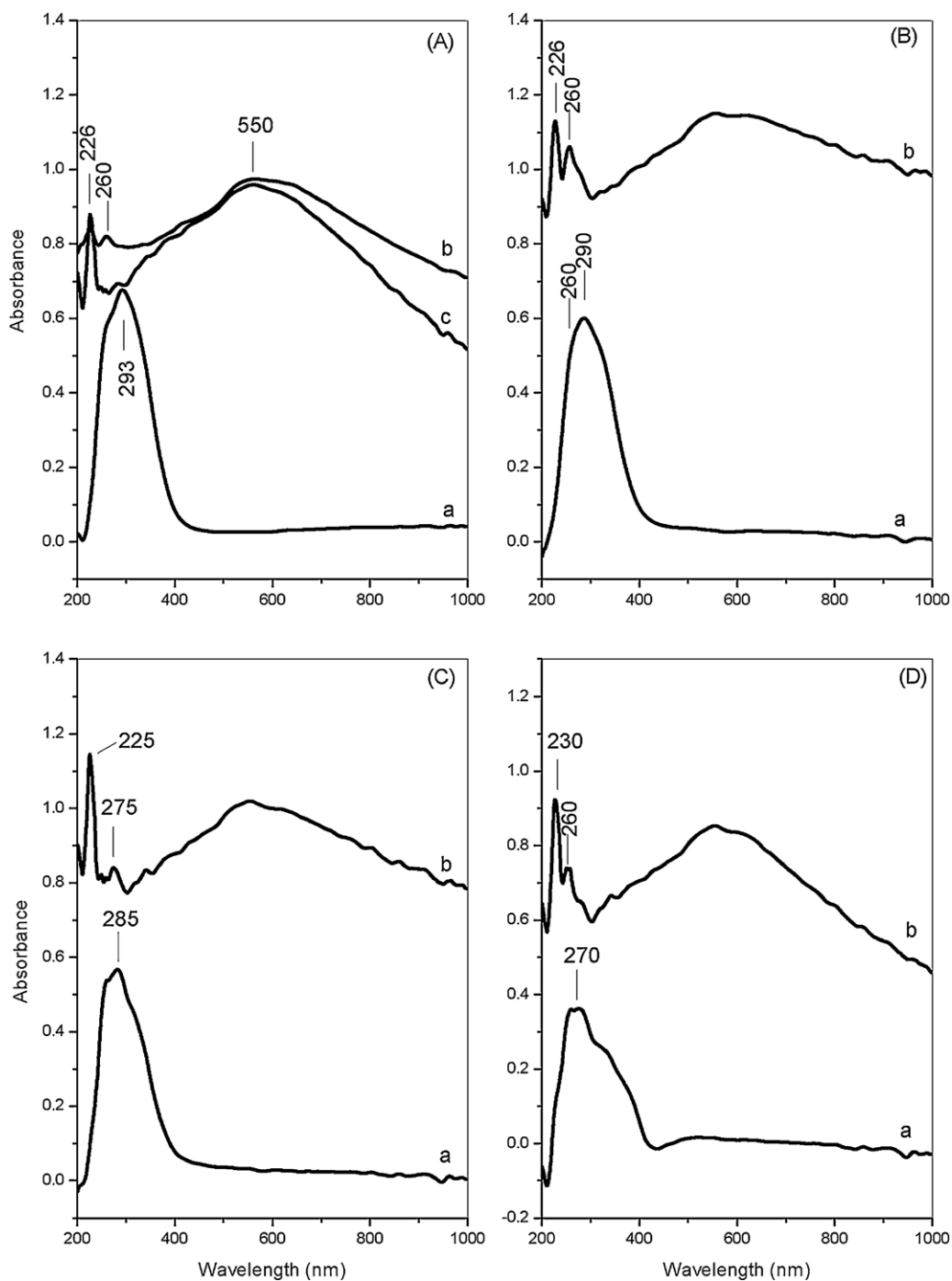
Fig. 2. (Panel A) Optical spectra of 18WZ-CP (a), Au/18WZ-CP (b) and Au/ZrO₂ (c). (Panel B) Optical spectra of 20WZ-I (a) and Au/20WZ-I (b). (Panel C) Optical spectra of 12WZ-I (a) and Au/12WZ-I (b). (Panel D) Optical spectra of 5WZ-I (a) and Au/5WZ-I (b).

Table 2
Binding energies, surface composition and gold particle size for the samples.

Sample	O 1s		Zr 3d$_{5/2}$		W 4f$_{7/2}$		Au 4f$_{7/2}$			Au particle size (nm)
	BE (eV)	at%	BE (eV)	at%	BE (eV)	at%	BE (eV)	at%	FWHM[a]	
Au/ZrO₂	530.2	65.2	182.5	34.6	–	–	82.8	0.2	2.03	2.6
Au/5WZ-I	530.0	63.3	182.1	35.3	35.1	1.2	82.8	0.2	1.87	2.9
Au/12WZ-I	530.5	63.5	182.6	33.9	35.8	2.3	83.0	0.3	1.88	2.8
Au/20WZ-I	530.6	63.0	182.6	33.0	35.9	3.7	83.4	0.3	1.71	3.1
Au/18WZ-CP	530.4	64.7	182.9	32.4	36.3	2.6	83.5	0.3	1.68	3.3

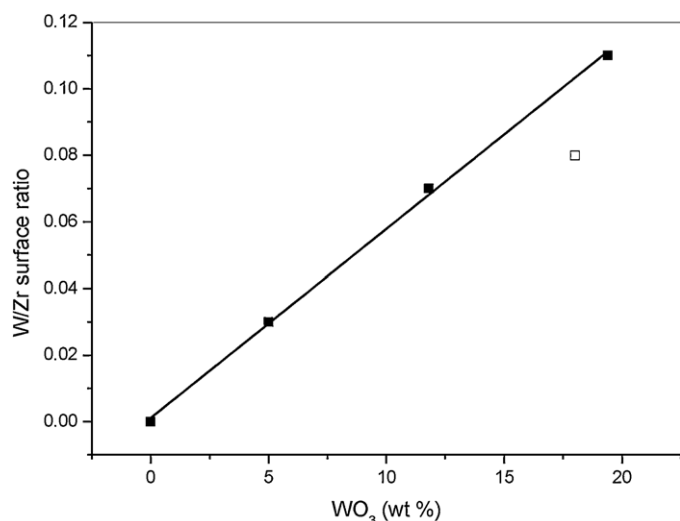[a] FWHM for the Au 4f$_{7/2}$ of metallic gold is 1.18 eV.

Fig. 3. W/Zr surface ratios as a function of WO_3 content in Au/xWZ-I (x = 0, 5, 12 and 20 wt% WO_3) (■) and Au/18WZ-CP samples (□).

hydroxyls of W-containing supports in the deposition process of gold precursor.

3.4.2. Adsorption of CO at room temperature

The analysis of the FT-IR spectra of CO adsorbed at room temperature on the samples can be very useful to obtain qualitative information on the nature of supported gold species. Fig. 5A displays the FT-IR spectra in the carbonyl region of CO (10 Torr) adsorbed on the zirconia samples obtained after the calcination at 600 °C of hydrated zirconias prepared by procedures 1 and 2. The figure shows also the spectra of CO adsorbed on the calcined supports prepared by impregnating the HZ-1 precursor with AMT solution and by coprecipitation. As mentioned above, the samples

of zirconia obtained using as precursors hydrated zirconias HZ-1 and HZ-2 crystallize after the calcination at 600 °C in monoclinic and tetragonal structure, respectively. A strong band at 2196 cm^{-1} with a poorly resolved shoulder is observed in the spectrum of CO adsorbed on monoclinic zirconia (Fig. 5A) which correspond to two types of Zr^{4+}—CO carbonyls [2,17,20,23,31,43–45]. For the pure tetragonal zirconia sample the CO adsorption yields also one asymmetric band at 2194 cm^{-1} with shoulder at around 2188 cm^{-1} which are ascribed to two types of Lewis acid sites [23,46]. The spectra clearly show that the population of the coordinatively unsaturated (cus) Zr^{4+} sites on monoclinic zirconia is larger than on the tetragonal zirconia. This experimental fact is in agreement with the results of Morterra and coworkers [23] who concluded that morphological and structural reasons are responsible for the different concentration of (cus) Zr^{4+} sites on the surfaces of the two crystallographic modifications of zirconia. Compared to the m-ZrO_2, the tungstated samples prepared from the HZ-1 precursor are characterized by lower intensity of the Zr^{4+}—CO band (Fig. 5B) due to saturation of coordinative positions of Zr^{4+} ions in the surface layer by the WO_x species. The intensity of the Zr^{4+}—CO band decreases gradually with increase in the tungsten loading. The high-frequency shift of the carbonyl band exhibited in the WO_x-containing zirconia samples is associated with the increased acidity of the (cus) Zr^{4+} sites caused by the electron-withdrawing WO_x groups [17,20]. The intensity of the Zr^{4+}—CO band in all xWZ-I samples (having a tetragonal structure) is significantly higher than that in the tetragonal zirconia. This difference can be ascribed to the application of two different procedures for the preparation of the hydrated zirconia used as precursor leading to different morphology of the t-ZrO_2 and xWZ-I samples, i.e. different size and shape of the particles, and different amounts of structural defects. In addition, the acidity of the (cus) Zr^{4+} ions located in the proximity of the WO_x domains is enhanced resulting in increased amount of (cus) Zr^{4+} ions detectable by CO adsorption at room temperature.
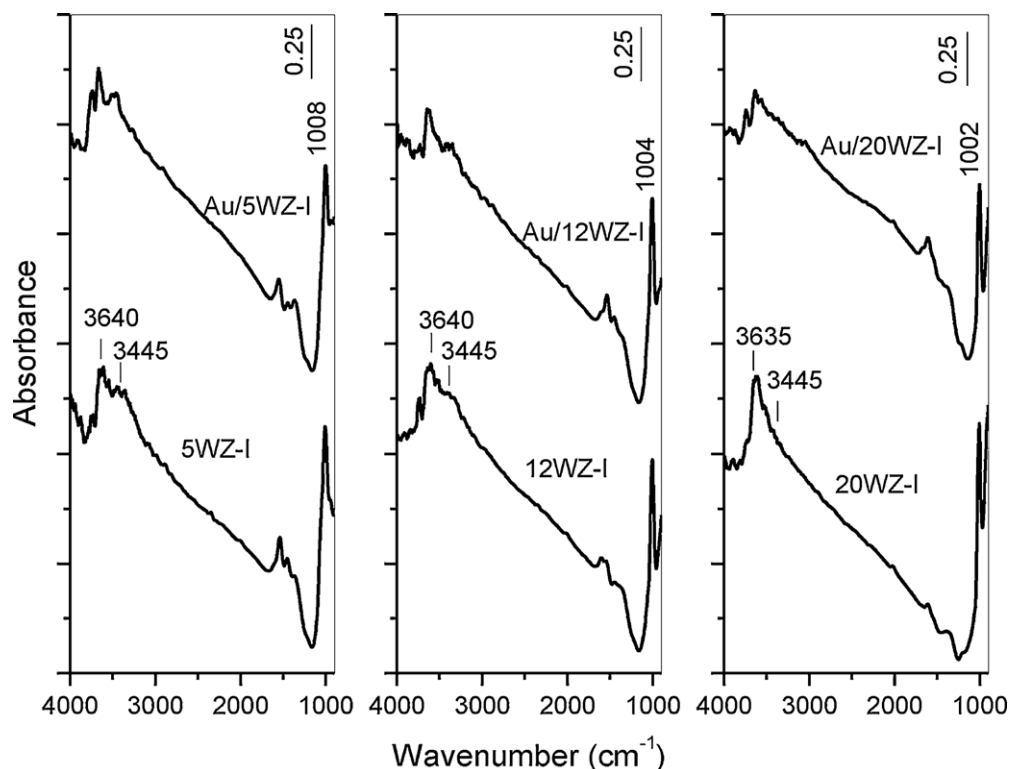

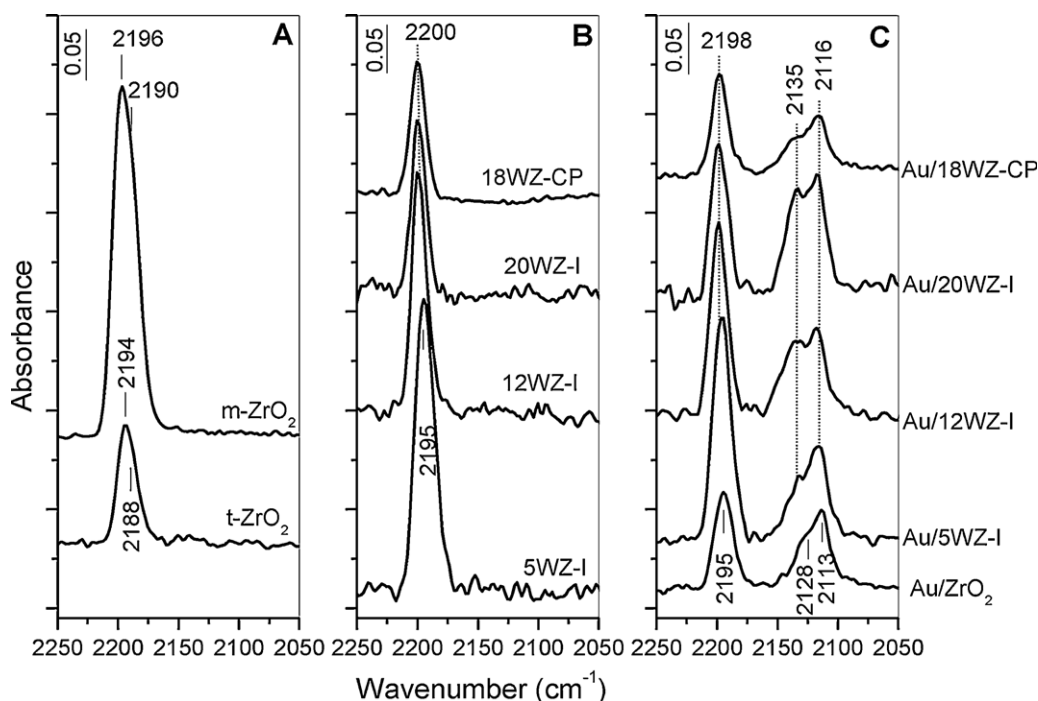**Fig. 4.** FT-IR spectra of the activated samples.

Fig. 5. FT-IR spectra of CO (10 Torr) adsorbed at room temperature on the samples studied (t: tetragonal; m: monoclinic).

As with the Au-free materials, the absorption at 2195–2198 cm^{-1} observed for all Au-promoted samples is assigned to CO adsorbed on Zr^{4+} surface sites (Fig. 5C). The intensity of the Zr^{4+}–CO band in the W-containing samples decreases after the deposition of gold (compare with Fig. 5B) indicating that there are gold nanoparticles located on the zirconia surface. Lower concentration of the (cus) Zr^{4+} ions has been detected also on the surface of Au/ZrO$_2$ sample as compared with the Au-free tetragonal zirconia. According to data from the literature [2,10,31,43,44,47–51], the absorption with maximum at 2113–2116 cm^{-1} is assigned to CO adsorbed on small three-dimensional gold clusters, whereas the shoulder at 2128–2135 cm^{-1} is usually attributed to Au$^{\delta+}$–CO species. Formation of positively polarized gold on ZrO$_2$ is assumed to be caused by the presence of adsorbed oxygen on the gold particles or their interaction with the support [2,31,43,47]. It should be noted that the last activation step of the investigated samples consisted of evacuation at 400 °C and adsorbed oxygen cannot be expected under these conditions. Moreover, after the reduction of the samples at 400 °C with CO, the absorption at 2128–2135 cm^{-1} is still present in the spectra of CO adsorbed at room temperature. Recently, absorption band at 2130–2140 cm^{-1} observed during the CO adsorption on Au/Nb$_2$O$_5$ has been attributed to CO coordinated to larger gold nanoparticles [52]. Therefore, based on the latter interpretation the feature at 2128–2135 cm^{-1} (Fig. 5C) is assigned tentatively to CO coordinated to larger gold nanoparticles. This proposition is supported by the estimates of gold particle sizes from XRD and XPS data showing that the samples have at least two fractions of crystallites, large (∼8–10 nm) and small (∼3 nm). For convenience, the absorptions at 2128–2135 cm^{-1} and 2113–2116 cm^{-1} are denoted as high-frequency (HF) and low-frequency (LF) gold carbonyls, respectively. The bands corresponding to the Zr^{4+}–CO and Au–CO species are removed upon dynamic evacuation at room temperature.

According to the chemical analysis the Au loading on Au/ZrO$_2$ and Au/5WZ-I samples is very close, 1.43 and 1.27 wt%, respectively. However, the intensities of the bands due to CO adsorbed on the gold sites are higher for the W-containing sample (Fig. 5C) suggesting higher gold dispersion. Using the same arguments (Au loading

and intensities of the Au carbonyl bands), better gold dispersion can be deduced for the Au/20WZ-I (2.06 wt% Au) when compared with the Au/18WZ-CP sample (2.27 wt% Au). The spectra of CO adsorbed on the Au-free supports show that the amount of (cus) Zr^{4+} ions is higher on the 5WZ-I sample than on t-ZrO$_2$. Likewise, the surface concentration of (cus) Zr^{4+} ions on the 20WZ-I sample is higher than that on the 18WZ-CP sample. It can be proposed that the dispersion of gold depends on the amount of (cus) Zr^{4+} ions. This assumption can be supported by the results of Chen and Goodman [53] who showed by using HREELS and CO adsorption that Au bonds directly to coordinatively unsaturated Ti atom on TiO$_2$ (1 1 0).

For the Au/xWZ-I sample series, the increase in the intensities of Au carbonyl bands with the amount of tungsten is associated with the increase in the Au loading. According to the results of curve fitting of the gold carbonyl bands (Table 3), the fraction of larger gold particles giving rise to the HF carbonyl band increases with the W loading by larger extent than the fraction of the smaller gold particles characterized by the LF carbonyl band. This experimental fact could be explained by the assumption that in the case of W-containing samples the gold particles formed during the calcination occupy preferentially the WO$_x$-free zirconia surface. The modification of zirconia by tungsten facilitates the gold uptake but at the same time causes decrease in the concentration of (cus) Zr^{4+} ions. The decrease in the amount of nucleation sites for gold particles with increase in the W loading lowers the dispersion.

Table 3
Integrated areas of the gold carbonyl bands recorded at room temperature and P_{CO} = 10 Torr (see Fig. 5).

Sample	HF band[a] (cm^{-1})	I_{HF} (a.u.)	LF band[b] (cm^{-1})	I_{LF} (a.u.)	I_{HF}/I_{LF}
Au/ZrO$_2$	2128	0.78	2113	0.97	0.80
Au/5WZ-I	2132	1.28	2115	1.35	0.95
Au/12WZ-I	2136	1.79	2116	1.38	1.30
Au/20WZ-I	2136	2.66	2116	1.53	1.74
Au/18WZ-CP	2134	0.84	2115	0.73	1.15

[a] HF band corresponds to CO adsorbed on large Au particles.
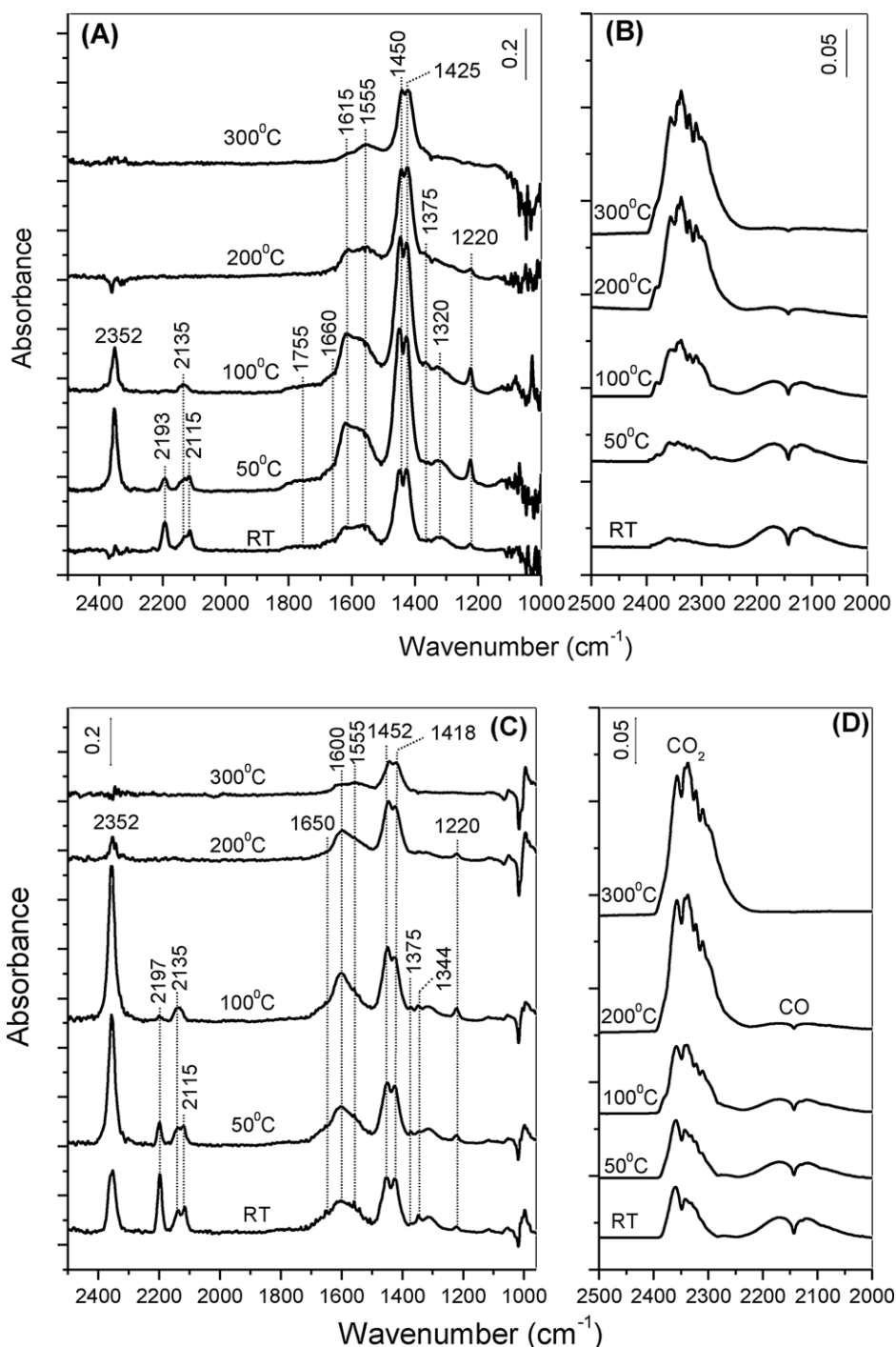[b] LF band corresponds to CO adsorbed on small gold particles.

Fig. 6. FT-IR spectra collected during the exposure of the samples Au/ZrO_2 (Panel A) and Au/12WZ-I (Panel C) to a (10 Torr CO + 10 Torr O_2) gas mixture for 10 min at various temperatures. (Panels B and D) Gas phase spectra above the Au/ZrO_2 and Au/12WZ-I samples, respectively (RT = room temperature).

3.4.3. FT-IR spectroscopic investigation of CO oxidation over Au/xWZ-I samples

In order to evaluate the potential of a new material as a catalyst, we studied by FT-IR spectroscopy the CO oxidation as a size sensitive probe reaction. In this investigation we used the gold catalysts supported on tungstated zirconia prepared by impregnation. In order to find information about the effect of tungsten, the CO + O_2 reaction has been studied on the Au/ZrO_2 sample as well. Fig. 6

Table 4
Assignment of the IR absorption bands observed upon CO + O_2 adsorption on Au/ZrO_2 and Au/12WZ-I samples at various temperatures.

IR band (cm^{-1})	Assignment	IR band (cm^{-1})	Assignment
2352, 1344	Zr—O—C—O	1660–1650, 1375	CO_2^-
2193–2197	Zr^{4+}—CO	1615, 1220	Bidentate HCO_3^-
2135, 2115	$Au^{\delta+}$—CO, Au^0—CO	1555, 1320	Bidentate CO_3^{2-}
1755	Bridged CO_3^{2-}	1452–1450, 1425–1418	Polydentate CO_3^{2-}

shows the spectra obtained during the contact of the Au/ZrO_2 and Au/12WZ-I catalysts with a $(10\,Torr\,CO + 10\,Torr\,O_2)$ mixture in the isolated IR cell at various temperatures for 10 min. The spectrum of Au/ZrO_2 catalyst detected at room temperature (spectrum RT in Fig. 6A) contains absorptions at 2193, 2135 and 2115 cm^{-1} the former band being assigned to Zr^{4+}—CO whereas the latter two bands correspond to HF and LF gold carbonyls, respectively. The spectrum in the 1620–1000 cm^{-1} region is similar to that reported by Bachiller-Baeza et al. [54], Pokrovski et al. [55] and Bolis et al. [56] for CO_2 adsorbed on tetragonal zirconia. Accordingly, the peaks at 1615 and 1220 cm^{-1} reveal the presence of bidentate hydrogencarbonates (b-HCO_3^-). The bands at 1555 and 1320 cm^{-1} are attributed to bidentate carbonate species (b-CO_3^{2-}) [54–56] and the pair of bands at 1450 and 1425 cm^{-1} are assigned to polydentate carbonates (p-CO_3^{2-}) [54,55] or monodentate carbonate species peculiar of the t-ZrO_2 phase [56]. The latter two bands are detected upon the adsorption of CO (10 Torr) at room temperature although with much weaker intensities. The absorption centered at 1755 cm^{-1} can be assigned to bridged CO_3^{2-} [56,57], whereas the weak bands at 1660–1650 and 1375 cm^{-1} (see also Fig. 6C) are attributed to carboxylate, CO_2^-, species [57–59]. In the gas phase, in addition to the signal of CO, very weak absorption corresponding to CO_2 is detected (Fig. 6B, spectrum RT). The experimental data show that some oxidation of CO takes place at room temperature. However, the product of oxidation is retained on the surface of the catalyst mainly as carbonate–carboxylate structures. Increasing the temperature to 50 °C causes enhancement of the absorptions between 1800 and 1000 cm^{-1} and decrease in the intensities of the carbonyl bands (Fig. 6A, spectrum 50 °C). At the same time, the formation of a new sharp band at 2352 cm^{-1} is observed. This signal is attributed to the ν_3 mode of CO_2 molecule linearly adsorbed on the surface Zr cationic sites through one O atom [56,58,59], i.e. to the Zr—O—C—O configuration. Increasing the temperature to 100 °C does not affect the intensities of the bands of the p-CO_3^{2-} species at 1450–1425 cm^{-1} (Fig. 6A, spectrum 100 °C). However, there is considerable decrease in the absorptions corresponding to adsorbed CO_2 (2352 cm^{-1}), b-HCO_3^- (1615 and 1220 cm^{-1}) and b-CO_3^{2-} species (1555 and 1320 cm^{-1}). Decrease in the intensities of the broad signal centered at 1755 cm^{-1} and the shoulder at 1660 cm^{-1} is observed as well. The bands at 2193 (Zr^{4+}—CO) and 2115 cm^{-1} (LF Au carbonyl) are no longer present. However, the species characterized by the HF Au carbonyl band display higher stability and are observed in the spectrum taken at 150 °C (not shown here). This indicates that CO adsorbed on the larger gold particles (giving rise to the band at 2135 cm^{-1}) is less reactive than that coordinated to the smaller gold clusters. Low reactivity of gold species characterized by carbonyl bands at 2125–2140 cm^{-1} has been reported for other gold containing samples [2,31,43].

The gas phase spectrum taken at 100 °C (Fig. 6B) shows decrease in the intensity of the CO band and significant increase in the amount of CO_2 produced. Further raise in the temperature to 200 and 300 °C causes vanishing of the bands at 1755 and 1660 cm^{-1} and the absorptions due to adsorbed CO_2 and CO, and lowering of the surface concentration of the hydrogencarbonate and carbonate species. Under these conditions the CO in the gas phase has almost disappeared and the amount of CO_2 formed has increased significantly.

The spectra obtained during the interaction of a (10 Torr $CO + 10\,Torr\,O_2$) mixture in the 25–300 °C with the Au/12WZ-I catalyst (Fig. 6C and D) contain the same type of absorption bands as those observed on the Au/ZrO_2 sample. However, there are differences that should be noted: (i) CO_2 adsorbed on the Au/12WZ-I sample is observed already at room temperature and the amount of CO_2 produced at 25 °C is significantly higher than that in the case of the Au/ZrO_2 sample. The larger concentration of CO_2 adsorbed on the Au/12WZ-I sample allows the detection of the ν_1 mode
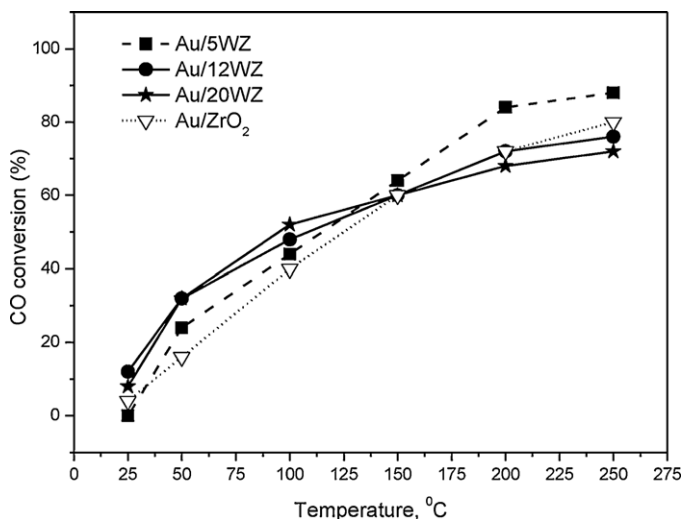

Fig. 7. CO conversion over the Au/xZW-I and Au/ZrO_2 catalysts as a function of the temperature. The CO conversion (in %) is estimated from the integrated area of the IR absorption of gaseous CO obtained at a given temperature in the presence (A) and absence of a catalyst (A_0) according to the equation: CO conversion (%) = ($A_0 - A$)100/A_0.

of the adsorbed molecule at 1344 cm^{-1}, otherwise IR inactive for gas-phase CO_2; (ii) between 25 and 100 °C there is approximately 2.5-fold increase in the surface concentration of adsorbed CO_2 whereas the amount of surface HCO_3^- and CO_3^{2-} increases only slightly and is much lower than that on the Au/ZrO_2 sample. This fact reflects the reduced basicity of the oxide ions of zirconia caused by the deposited WO_x species. CO_2 is acidic and it is used as a probe molecule for basic surface sites [54,56]. The assignment of the absorption bands is summarized in Table 4.

It should be pointed out that Au-free WO_x—ZrO_2 samples do not catalyze the oxidation of CO in the 25–300 °C temperature range under the same partial pressures of the reacting gases. Fig. 7 shows the CO conversion over the Au/xZW-I and Au/ZrO_2 catalysts as a function of the temperature. The CO conversion (in %) is estimated from the integrated area of the IR absorption of gaseous CO obtained at a given temperature in the presence (A) and absence of a catalyst (A_0) according to the equation: CO conversion = ($A_0 - A$)100/A_0. The curves clearly indicate that under the conditions of the FT-IR experiment, the Au/ZrO_2 catalyst displays the lowest activity in the low-temperature range (up to 150 °C). The behavior of the latter sample can be explained by extensive formation of surface HCO_3^-/CO_3^{2-} structures (see Fig. 6A) that block the active sites for the reaction. The amount of carbonates retained on the surface depends on the basicity of the oxide ions, i.e. on the W concentration. The spectra in Fig. 6A and C show that the most resistant to decomposition are the p-CO_3^{2-} species and their surface concentration decreases with the increase in the W content.

The Au/5WZ-I sample has the best high-temperature activity (above 150 °C) among the samples studied. The poorer performance of the gold catalysts with WO_3 loading of 12 and 20 wt% under these conditions could be explained by the presence of significant amount of large gold particles (see Table 3). The reactivity of CO adsorbed on large gold clusters is low resulting in lower CO oxidation activity. As mentioned above, both Au/ZrO_2 and Au/5WZ-I catalysts have similar Au loading and the fraction of small gold particles is comparable (Table 3). The lower activity of the Au/ZrO_2 catalyst than that of Au/5WZ-I could be attributed to the presence of stable HCO_3^-/CO_3^{2-} structures which are accumulated at temperatures below 150 °C and cannot be removed even at 300 °C. The results obtained indicate that gold catalysts supported on tungstated zirconia show low-temperature activity in the oxidation of CO. However,

the deposition of gold on tungstated zirconia by adsorption of $[Au(en)_2]^{3+}$ complex leads to the formation of non-uniform in size gold crystallites i.e. large and small. Since the size of gold particles is a key feature determining the activity in CO oxidation, our future task is to optimize the process of gold deposition by application of other methods such as using colloidal gold precursors or post-modification of Au/ZrO_2 by WO_x species.

4. Conclusions

We have shown that gold catalysts supported on tungstated zirconia (containing 5–20 wt% WO_3) can be prepared by cationic adsorption from aqueous solution of $[Au(en)_2]Cl_3$ complex. According to XRD and XPS data large (8–10 nm) and small ($\sim$3 nm) gold particles are present on the catalyst surfaces. The FT-IR spectra of adsorbed CO show the formation of two types of Au–CO bands, at 2128–2135 cm^{-1} (high-frequency band) and 2113–2116 cm^{-1} (low-frequency band), which are attributed to CO coordinated to large and small gold particles, respectively. It is concluded that the gold particles occupy preferentially the WO_x-free zirconia surface and the dispersion of gold depends on the amount of coodinatively unsaturated (cus) Zr^{4+} ions. Modification of zirconia by tungsten increases the gold uptake but at the same time causes decrease in the concentration of (cus) Zr^{4+} ions. Consequently, the fraction of large gold particles increases. Under the conditions of the FT-IR experiments, the gold catalysts supported on tungstated zirconia prepared by impregnation display higher activity in the CO oxidation in the low-temperature range (up to 150 °C) than the WO_x-free Au/ZrO_2 catalyst. The improved performance of the Au/WO_x–ZrO_2 catalysts is associated with reduced formation of stable HCO_3^-/CO_3^{2-} structures that block the active sites for the reaction.

Acknowledgments

References

[1] M. Haruta, CATTECH 6 (2002) 102–115.
[2] J.-D. Grunwald, M. Macviejewski, O.S. Becker, P.F. Fabrizioli, A. Baiker, J. Catal. 186 (1999) 458–469.
[3] P. Konova, A. Naydenov, Cv. Venkov, D. Mehandjiev, D. Andreeva, T. Tabakova, J. Mol. Catal. A 213 (2004) 235–240.
[4] P. Konova, A. Naydenov, T. Tabakova, D. Mehandjiev, Catal. Commun. 5 (2004) 537–542.
[5] D. Widmann, Y. Liu, F. Schüth, R.J. Behm, J. Catal. 276 (2010) 292–305.
[6] A. Knell, P. Barnickel, A. Baiker, A. Wokaun, J. Catal. 137 (1992) 306–321.
[7] X. Zhang, H. Wang, B.-Q. Xu, J. Phys. Chem. B 109 (2005) 9678–9683.
[8] H.G. Zhu, C.D. Liang, W.F. Yan, S.H. Overbury, S. Dai, J. Phys. Chem. B 110 (2006) 10842–10848.
[9] H.G. Zhu, Z. Ma, J.C. Clark, Z.W. Pan, S.H. Overbury, S. Dai, Appl. Catal. A 326 (2007) 89–99.
[10] D. Guillemot, V. Yu Borovkov, V.B. Kazansky, M. Polisset-Thfoin, J. Fraissard, J. Chem. Soc. Faraday Trans. 93 (1997) 3587–3591.
[11] R. Zanella, A. Sandoval, P. Santiago, V.A. Basink, J.M. Saniger, J. Phys. Chem. B 110 (2006) 8559–8565.
[12] J. Xu, Y. Liu, H. Wu, X. Li, M. He, P. Wu, Catal. Lett. 141 (2011) 860–865.
[13] J.G. Santiesteban, J.V. Vartuli, S. Han, R.D. Bastian, C.D. Chang, J. Catal. 168 (1997) 431–441.
[14] A. Martinez, G. Prieto, M.A. Arribas, P. Concepcion, J.F. Sanchez-Royo, J. Catal. 248 (2007) 288–302.
[15] B.P. Block, J.C. Bailar Jr., J. Am. Chem. Soc. 73 (1951) 4722–4725.
[16] R.A. Boyse, E. Ko, J. Catal. 171 (1997) 191–207.
[17] M. Scheithauer, R.K. Grasselli, H. Knozinger, Langmuir 14 (1998) 3019–3029.
[18] D.G. Barton, M. Shtein, R.D. Wilson, S.T. Soled, E. Iglesia, J. Phys. Chem. B 103 (1999) 630–640.
[19] E.I. Ross-Medgaarden, W.V. Knowles, T. Kim, M.S. Wong, W. Zhou, C.J. Kiely, I.E. Wachs, J. Catal. 256 (2008) 108–125.
[20] M. Kantcheva, C. Koz, J. Mater. Sci. 42 (2007) 6074–6086.
[21] E.I. Ross-Medgaarden, I.E. Wachs, J. Phys. Chem. C 111 (2007) 15089–15099.
[22] F. Di Gregorio, V. Keller, J. Catal. 225 (2004) 45–55.
[23] V. Bolis, G. Cerrato, G. Magnaca, C. Morterra, Thermochim. Acta 312 (1998) 63–77.
[24] K.T. Jung, A.T. Bell, J. Mol. Catal. A 163 (2000) 27–42.
[25] J. Li, J. Chen, W. Song, J. Liu, W. Shen, Appl. Catal. A 334 (2008) 321–329.
[26] C.E. Crouthamel, C.E. Johnson, Anal. Chem. 26 (1954) 1284–1291.
[27] D.F. Wood, R.T. Clark, Analyst 83 (1958) 326–334.
[28] F.P.J.M. Kerkhof, J.A. Moulijn, J. Phys. Chem. 83 (1979) 1612–1619.
[29] V. Leon, Surf. Sci. 339 (1995) L931–L934.
[30] M.A. Cortes-Jacome, C. Angeles-Chavez, E. Lopez-Salinas, J. Navarrete, P. Toribo, J.A. Toledo, Appl. Catal. A 318 (2007) 178–189.
[31] F. Boccuzzi, G. Cerrato, F. Pinna, G. Strukul, J. Phys. Chem. B 102 (1998) 5733–5736.
[32] R. Kydd, J. Scott, W.Y. Teoh, K. Chiang, R. Amal, Langmuir 26 (2010) 2099–2106.
[33] S. Eustis, M.A. El-Sayed, Chem. Soc. Rev. 35 (2006) 209–217.
[34] Y. Azizi, C. Petit, V. Pitchon, J. Catal. 269 (2010) 26–32.
[35] S. Schimpf, M. Lucas, C. Mohr, U. Rodemerck, A. Bruckner, J. Radnik, H. Hofmeister, P. Claus, Catal. Today 72 (2002) 63–78.
[36] L. Ilieva, J.W. Sobczak, M. Manzoli, B.L. Su, D. Andreeva, Appl. Catal. A 291 (2005) 85–92.
[37] R. Zanella, L. Dellanoy, C. Louis, Appl. Catal. A 291 (2005) 62–72.
[38] R. Wojciszek, M.J. Genet, P. Eloy, P. Ruiz, E.M. Gaigneaux, J. Phys. Chem. 114 (2010) 16677–16684.
[39] S. Velu, K. Suzuki, C.S. Gopinath, H. Yoshidac, T. Hattori, Phys. Chem. Chem. Phys. 4 (2002) 1990–1999.
[40] L.-C. Wang, Q. Liu, M. Chen, Y.-M. Liu, Y. Cao, He-Y. He, K.-N. Fan, J. Phys. Chem. C 111 (2007) 16549–16557.
[41] R. Grabowski, J. Sloczynski, M. Sliwa, D. Mucha, R.P. Socha, ACS Catal. 1 (2011) 266–278.
[42] J.C. Dupin, D. Gonbeau, P. Vinatier, A. Levasseur, Phys. Chem. Chem. Phys. 2 (2000) 1319–1324.
[43] M. Maciejewski, P. Fabrizioli, J.-D. Grunwald, O.S. Becker, A. Baiker, Phys. Chem. Chem. Phys. 3 (2001) 3846–3855.
[44] M. Manzoli, A. Chiorino, F. Boccuzzi, Surf. Sci. 532–535 (2003) 377–382.
[45] M. Kantcheva, E.Z. Ciftlikli, J. Phys. Chem. B 106 (2002) 3941–3949.
[46] C. Morterra, G. Cerrato, V. Bolis, C. Lamberti, L. Ferroni, L. Montanaro, J. Chem. Soc. Faraday Trans. 91 (1995) 113–123.
[47] F. Boccuzzi, A. Chiorino, J. Phys. Chem. B 104 (2000) 5414–5416.
[48] K.I. Hadjiivanov, G.N. Vayssilov, Adv. Catal. 47 (2002) 307–511.
[49] M. Kantcheva, O. Samarskaya, L. Ilieva, G. Pantaleo, A.M. Venezia, D. Andreeva, Appl. Catal. B 88 (2009) 113–126.
[50] D. Andreeva, M. Kantcheva, I. Ivanov, L. Ilieva, J.W. Sobczak, W. Lisowski, Catal. Today 158 (2010) 69–77.
[51] F. Vindigni, M. Manzolli, A. Chiorino, F. Boccuzzi, Gold Bull. 42 (2009) 106–112.
[52] K. Musialska, E. Finocchio, I. Sobczak, G. Busca, R. Wojcieszak, E. Gaigneaux, M. Ziolek, Appl. Catal. A 384 (2010) 70–77.
[53] M.S. Chen, D.W. Goodman, Science 306 (2004) 252–255.
[54] B. Bachiller-Baeza, I. Rodriguez-Ramos, A. Guerrero-Ruiz, Langmuir 14 (1998) 3556–3564.
[55] K. Pokrovski, K.T. Jung, A.T. Bell, Langmuir 17 (2001) 4297–4303.
[56] V. Bolis, G. Magnacca, G. Cerrato, C. Morterra, Top. Catal. 19 (2002) 259–269.
[57] G. Busca, V. Lorenzelli, Mater. Chem. 7 (1982) 89–126.
[58] G. Ramis, G. Busca, V. Lorenzelli, Mater. Chem. Phys. 29 (1991) 425–435.
[59] L.F. Liao, C.F. Lien, D.L. Shieh, M.T. Chen, J.L. Lin, J. Phys. Chem. B 106 (2002) 11240–11245.